Title
Field observations and numerical model experiments for the snowmelt process at a field site

Journal
Advances in Water Resources, 29(2)

ISSN
0309-1708

Authors
Ohara, N
Kawas, M L

Publication Date
2006-02-01

Peer reviewed

Available online at www.sciencedirect.com
SCIENCE DIRECT®
Advances in Water Resources 29 (2006) 194–211
Advances in Water Resources
www.elsevier.com/locate/advwatres

Field observations and numerical model experiments for the snowmelt process at a field site

N. Ohara *, M.L. Kavvas

Hydrological Research Laboratory, Department of Civil and Environmental Engineering, University of California, One Shields Avenue, Davis, CA 95616, USA

Received 8 February 2005; accepted 11 March 2005
Available online 1 July 2005

Abstract

There are several levels of models for the snowmelt process in terms of the snow thermal structure: isothermal, bi-layered and multi-layered models. However, it is difficult to choose the appropriate level of complexity for application because the number of unknown variables is crucial in model handling. One of the major issues in energy balance snow models is the shape of the snow temperature vertical profile. This profile, if taken as a specified function, would simplify a snowmelt model calibration and computation significantly. In this study, in order to determine the appropriate representative snow vertical thermal profile, snow temperature measurements have been performed using five snow thermocouples placed vertically along an observation tower with insulating arms. Also, as a field experimental study of an energy balance snow model, the net radiation, air temperature, relative humidity and wind speed along with the vertical one dimensional snow temperature profile have been observed at a field site in Lake Tahoe Basin. The computational results correspond with the measured snow temperature profile and snow water equivalent reasonably well. It is illustrated that the temperature in the snow near surface (called the ''active layer'') varies daily, and the lower snow layer (called the ''inactive layer'') is barely affected by the atmosphere. The results of field observations and the numerical experiments show that the vertical temperature distributions in the active layer, which is the upper layer affected by energy exchange with the atmosphere, generally have an exponential shape during night time under cold weather, while snow pack stays around 0 °C during daytime. Both of the results indicate that not only the snow temperature in the top active layer, but also the thickness of snow active layer fluctuates during the snowmelt process. The observation results show that the thickness of the active layer may reach about 60 cm in Sierra Nevada, California. These results provide significant information for the development of appropriate approximations in physically based snowmelt modeling.

Keywords: Snowmelt; Snow temperature; Active layer; Field observation; Physically based model; Distributed snow model

1. Introduction

1.1. Background

A snowmelt runoff model is an important component of a watershed hydrology model since substantial amounts of precipitation water are stored in the snowpack and released in time from the pack in order to dictate the hydrologic regime in mountainous regions. Several snow models have been proposed and one may classify them in Table 1. At first, snowmelt models can be classified into two groups: conceptual models and physically based models. A degree-day method and Tank model are categorized under conceptual models, and an energy budget model may be classified as a physically based model. Another method for classification of snowmelt models is scaling. One can partition the

* Corresponding author.
E-mail addresses: nohara@ucdavis.edu (N. Ohara), mlkavvas@ucdavis.edu (M.L. Kavvas).

0309-1708/$ - see front matter © 2005 Elsevier Ltd. All rights reserved.
doi:10.1016/j.advwatres.2005.03.016

Table 1
Classification of snowmelt models

Conceptual models
- Degree-Day model (ACOE [40])
- Tank model (Sugawara [37])

Physically based models (Energy budget model)
Point-scale or 1D model
- Isothermal model (ACOE [40])
- Two-layer model (Marks et al. [27])
- Linear temperature model (Kondo and Yamazaki [23])
- Multiple layer model (Jordan [20])

Distributed model [Numerical upscaling]
- Distributed degree-day models (Dune and Colohan [11], and others)
- SHE (Isothermal model) (Abbott et al. [1], and others)
- ISNOBAL (Two-layer model) (Marks et al. [28])
- WEHY (Linear temperature model) (This study)

Stochastic model [Stochastic upscaling]
- Monte-Carlo model (Kuchment et al. [25])
- Regular perturbation model (Horne and Kavvas [17])
- Pdf model (Ohara [34])

models into three groups: point scale or depthwise 1D model, distributed model, and stochastic model.

Degree-day or temperature-index methods are empirical or can result from a linearization of the energy budget equation. In practice, the degree-day method has been widely used, because it is difficult in a whole watershed to obtain all the necessary meteorological data, such as dew point, amount of cloudiness, wind speed and short- and long-wave radiation, for an energy balance method. In this approach daily snowmelt is assumed proportional to the difference between average daily temperature and a base temperature. Although the degree-day method has empirical parts, it is applied to many situations because of its simplicity.

The US Army Corps of Engineers [40] developed a model based on processes of energy exchange between a snowpack and its environment. More recent energy balance models were developed by Anderson [2], Amorocho and Espildora [4], and others. This approach is categorized under physically based models. The amount of snowmelt can be predicted if the energy exchange through the snow surface can be estimated by means of the atmospheric data. The snowpack energy budget is written in terms of the energy flux to and from a snowpack, with units of energy per unit area per unit time. The components of energy budget are (1) change in heat storage within the snowpack, (2) net short-wave and long-wave radiation, (3) heat flux to snowpack from the underlying ground, (4) convective transport of sensible heat from the air to snowpack, (5) release of latent heat of vaporization and (6) advection of heat to snowpack by rainfall.

Recent developments in snow hydrology are mostly based upon energy balance framework. Morris [30,31] formulated general point-scale equations for the conservation of mass and energy within a snowpack in order to simulate snowmelt and water movement in the pack. Marks et al. [27] modeled a snowpack in terms of two layers since snow temperature in only the top part of the snowpack varied significantly in nature. Their model, called SNOBAL, was applied in many regions (e.g. California, Utah, and Idaho, USA) and performed satisfactorily in most cases. In order to achieve a realistic snow temperature description, an assumption of linear snow temperature profile was made by Kondo and Yamazaki [23]. They introduced the concept of freezing depth, a border between active and inactive layers of a snowpack that is calculated by snow temperature gradient at a snow surface. Their work will be discussed in detail later in this study. Moreover, Jordan [20] employed the general point scale equations to develop a multi-layered point location scale model, SNTHERM89. Obled and Rosse [33] and Blöschl and Kirnbauer [8] compared the performance of distributed and isothermal point location models. They concluded that the simpler isothermal model was able to perform satisfactorily in most situations. However, the isothermal model did not express internal processes properly during freeze-thaw cycles, while the detailed distributed model could perform well in all conditions.

In the detailed physically based distributed models, however, it is difficult to determine the initial structure of snowpack, and the computational demand becomes large in practice. With respect to heterogeneity, the variation of snow water content in the vertical direction within a snowpack is more uniform than the horizontal distribution of snow at the watershed scale. Hence, some researchers focused their efforts on the effect of heterogeneity on the snowmelt process. There are two major approaches to upscaling from the point scale to the finite areal scale: spatially distributed model (numerical upscaling) and stochastic model approach (stochastic upscaling). In the spatially distributed model approach, the point scale model is independently applied at every computational node of the grid network. On the other hand, the stochastic model approach computes the ensemble average of the stochastic state variables with the effects of spatial heterogeneities of atmospheric and topographic conditions in a finite area. For describing spatial heterogeneity of state variables, the spatially distributed snow model has been the popular approach in the last couple of decades. Abbott et al. [1] introduced distributed isothermal energy balance model as a snow component in the European Hydrological System (SHE) model. Marks et al. [28] developed another spatially distributed snowmelt model, called ISNOBAL, based on the GIS and satellite information. They approximated the snow pack in two layers: active (top)

and inactive (bottom) layer. Since a lot of computation has to be done in the grid-based or numerical upscaling approach, a stable, quick and reliable point scale model is required as an engine in the distributed snow model.

The motivation of this study is to find out which point scale model is the most appropriate for spatially distributed modeling of snowmelt through the analyses of the vertical snow thermal behavior with the field observations and numerical experiments. In order to monitor the thermal behavior of the snowpack, five thermo couples were mounted vertically along a tower at a field observation site in Ward Creek watershed in Lake Tahoe basin, California. Because the vertical distances among sensors were not sufficiently fine to represent a snow temperature profile very well, a snow temperature profile numerical modeling experiment was carried out as well. The time evolution of the snow temperature profile will be discussed in Section 2.

As an application, the linear temperature profile model will be introduced and examined. The original idea of the linear temperature model comes from Kondo and Yamazaki's framework [23]. Several important components to this framework were added (snow density evolution and snow accumulation), and its theoretical validation and numerical algorithm were improved. The developed linear temperature snow model has been tested at the Ward Creek observation station during a two-year period. The linear temperature model in point scale will be examined in Section 3.

Additionally, in Section 4, the linear temperature model has been expanded into a spatially distributed model with estimated short-wave radiation by a solar geometry method in order to demonstrate the performance of the developed model. The developed model is applied to an ungaged watershed to exhibit the advantages of the physically based approach.

1.2. Introduction of the field observation sites

In this section, two application fields in Sierra Nevada in Northern California are introduced. Ward Creek watershed has a small catchment area, and is well monitored. Upper Cosumnes River watershed is a large ungaged basin. The model presented here is applied to these two watersheds.

Ward creek watershed is located in Lake Tahoe basin of Northern California and has 26.4 km^2 catchment area. Most of the watershed is mountainous. The original vegetation was conifer forest but open space was created for skiing activity in some areas of the basin. Usually, a maximum of two to three meters of snow depth develops over the watershed during winter. There are several observation stations in Ward creek watershed. One of the meteorological stations provides hourly precipitation, air temperature, and snow water content data and the other offers only daily data for the above variables. Additionally, the authors monitor a field station at Ward Creek watershed for observing snowmelt, overland flow and subsurface flow. The data of this station are available starting 1998 at 15 min time intervals for air temperature, ground temperature, relative humidity, wind velocity, short-wave radiation, total radiation, and flow discharge from a hillslope surface and subsurface, from rills and from a cross-section of the South fork of Ward Creek. The snow temperature measurements are also implemented at the field observation station.

Upper Cosumnes River watershed represents an ungaged basin. The watershed has 1400 km^2 catchment area that is about ten times larger than Ward Creek watershed. East side of the watershed is mountainous and is covered with conifer forest. Usually, snowfall occurs in the mountainous region during winter. Basically, no field observation station is located in this watershed. The weather in this watershed needs to be estimated by the observed meteorological data, provided by neighboring weather stations or an atmospheric model. The weather stations near the watershed are Ben Bolt (BLT), Beaver (BVE), Mt. Zion (MTZ), and Owens Camp (OWC), operated by CDWR. Among these stations, since the data from Owens Camp has too many missing values during the simulation period, they were not used. In this study, the required meteorological data for each computational grid are spatially interpolated from data that were observed at the above-mentioned stations, using inverse distance method, in order to check the performance of the developed snowmelt model.

2. Snow temperature profile

2.1. Observation of snow temperature

A vertical snow temperature profile is affected by various complicated phenomena within a snowpack. As mentioned in the previous section, main energy exchanges take place at the top of snow cover while only short-wave radiation can penetrate snow near surface. As a result, snowmelt mostly occurs around snow surface. The snowmelt water obeys gravity and percolates into snow structure as unsaturated flow. The melted water conveys heat downward from the snow surface. Meanwhile, air convection between snow particles also brings heat toward the snow surface. During night, the penetrating water freezes, and it may cause rounding of snow particles and layering of snow structure. The snow temperature profile is not uniform most of the time, and is controlled by many different processes.

Field observations are the most direct way to monitor what happens to the temperature distribution within the snow pack. However, when a field observation is carried out, an observer always needs to pay attention to the

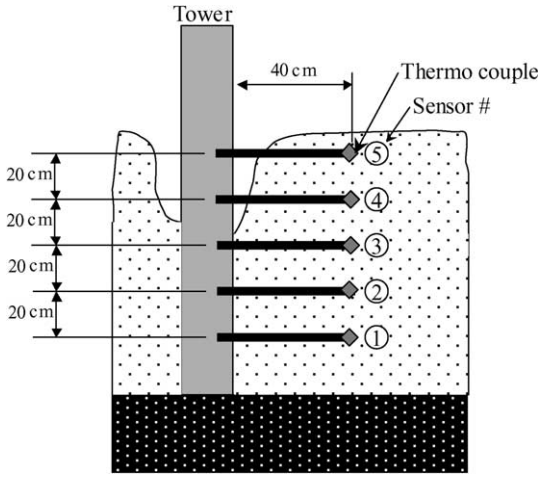

Fig. 1. A sketch of the field observation for snow temperature profile.

quality of the observed data and source of errors. In snow temperature observation, in fact, because thermo-couples are affected by solar radiation near the snow surface, the snow temperature data for the daytime are usually not reliable. Also, the sensors should be insulated from their suspension carefully because heat can be conducted through the tower and cables instead of snow. It is important for a data collector to manage the quality of observed data.

In January 2003, the first author installed five thermo-couples in snow in the vertical direction along a weather tower (shown in Fig. 1) in Ward Creek watershed, California. The five sensors were located at every 20 cm. The sensors are HOBO thermo-couple type T that has a measurement range from −200 °C to 50 °C, and a resolution in 0.1 °C. The weather tower absorbs more heat than snow because the tower has much less reflectance of radiation than snow has. In order to keep the sensors within the snow and minimize heat conduction from the tower to the sensors, narrow wood bars (40 cm) that have small heat conductivity were used as horizontal arms. Also, the horizontal arms effectively work to keep the probes in the snow pack because the snow around an object like the tower melts much faster than in other places.

Fig. 2 shows the time series plot of observed snow temperatures from March 30 to April 16, 2003. When the top probe (no. 5) is covered by snow, then the appropriate period to observe the time variation of the snow temperature profile starts. The darker color indicates deeper sensor in the snowpack in Fig. 2. The observed temperature frequently exceeded zero because of warm weather and solar radiation penetrating the snow structure in daytime. In order to clarify Fig. 2 for influences concerning snow temperature profile, the positive temperatures have been replaced by zero temperature because the snow thermal conditions that need to be modeled are mainly under the cold weather and night time conditions. Under cold weather during April 1–7, one can observe the typical behavior of snow temperature where snow temperature near the surface moves very far below zero during night time, while the snow temperature deep inside the snowpack does not move much. There are apparently two different regions with respect to depth within a snowpack: an active layer and an inactive layer. This may be the reason why major physically based snow models adopt two or more layers. It should be noted that the location of the border of active layer and inactive layer (freezing depth) varies in time. In other words, it may not be appropriate to consider the thickness of active layer as a constant.

Fig. 3 shows the observed snow temperature profile at every hour during the period April 3–7 in order to examine the evolution of snow temperature profile. The T_s in Fig. 3 indicates the snow temperature. This figure shows that the surface sensor no. 5 is very sensitive to energy exchange, and this exchange affects the deeper snow temperature later. According to Fig. 3, the snow temperature profile seems exponentially or linearly distributed most of the time. Fig. 3 implies that a linear temperature variation approximation seems to be much more reasonable than an isothermal two-layer approximation for snow vertical temperature distribution.

This field observation as shown in Fig. 3 yields a description of approximate but actual snow temperature behavior although it has large vertical intervals among sensors. In the next section, a one dimensional heat transfer model is introduced in order to resolve the

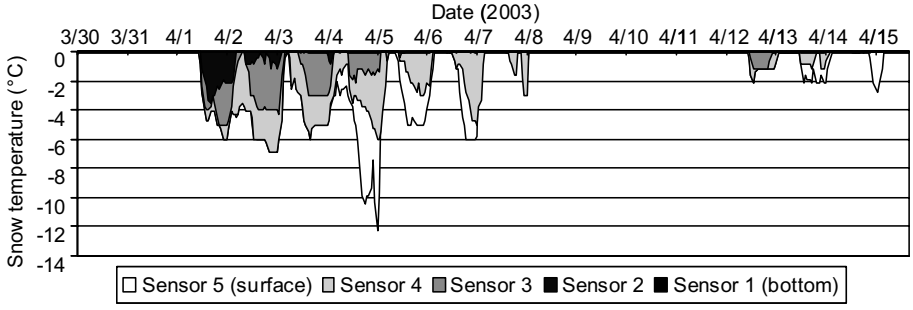

Fig. 2. Observed snow temperature at five different depths.

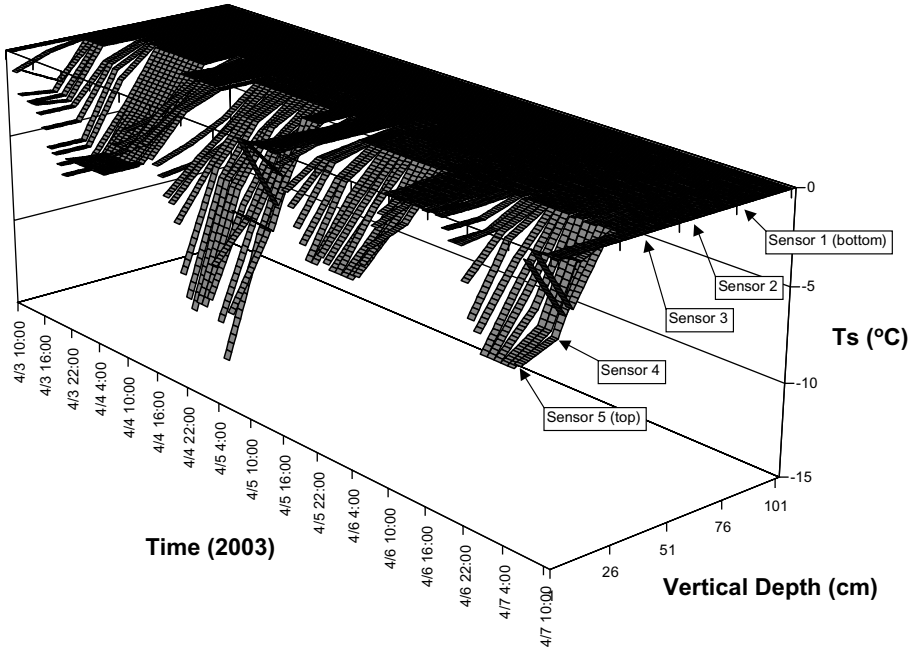

Fig. 3. Observed snow temperature profile at every hour from April 3 through April 7. T_s indicates snow temperature.

coarse spatial resolution in the vertical direction, and to understand this phenomenon better.

2.2. Numerical snow temperature model

A simple one dimensional heat transfer model is convenient for understanding the vertical heat distribution in a snow column. This model may be categorized under the multiple layer models. It may be noted that because this model does not accommodate snow water movement, variation of snow depth and effect of snow density change, this one-dimensional model cannot be applied for long-term simulation. However, the simple heat transfer model is a useful tool to obtain a description of a snow temperature profile for a short period.

The heat equation for a snow pack can be formulated easily by adding the energy exchange terms as forcing to a simple heat equation. In this study, the energy conservation equation, formulated by Kondo and Yamazaki [23], is used:

$$C_s\rho_s\frac{\partial T_s}{\partial t}=\lambda_s\frac{\partial^2 T_s}{\partial z^2}+\mu S_{net}\exp(-\mu z)-M,\quad z>0 \tag{1}$$

and at the top boundary (snow surface),

$$C_s\rho_s\frac{\partial T_s}{\partial t}\,\mathrm{d}z=\lambda_s\left(\frac{\partial T_s}{\partial z}\right)_{z=0}+\{\mu S_{net}\exp(-\mu z)-M\}\mathrm{d}z+L_{in}-L_{out}+H-lE,\quad z=0, \tag{2}$$

where z is distance from the snow surface (m), t is time (s), ρ_s is density of snow (kg/m^3) at depth z, T_s is snow temperature at depth z, S_{net} (kW) is net short-wave radiation, L_{in} and L_{out} (kW) are incoming and outgoing long-wave radiation, H (kW) is the sensible heat flux, lE (kW) is latent heat flux; C_s is specific heat of snow, λ_s is heat conductivity of snow, and μ is the extinction coefficient of solar radiation within the snow pack. Short-wave radiation penetrates a snow pack with an exponential decrease in the pack, although other energy components occur at the snow surface. The heat fluxes at the snow surface may be estimated from meteorological information (e.g. [14]). The mass conservation equation can be written as:

$$\frac{\partial \mathrm{WC}}{\partial t}=\frac{M_r}{\rho_s}-Q, \tag{3}$$

where WC is water content; M_r is snowmelt rate (m/s), and Q is discharge from the system (m/s). M_r (m/s) is determined by the snowmelt energy, M:

$$M_r=\frac{M}{L_f\rho_w(1-W_0)}. \tag{4}$$

Snow temperature and water content are the state variables for this system with the additional variable, snowmelt rate. Fig. 4 is a schematic of the snow cover that is used to compute the evolution of the vertical snow temperature profile. The system that consists of the energy equation, Eqs. (1) and (2), and the mass balance equation, Eq. (3), can be rewritten in finite difference form for each grid point. This system can be solved by an explicit finite difference scheme under the condition whether the snowmelt happens or not. The numerical algorithm for 1D temperature profile model is shown in Appendix A in detail.

The numerical model computations were carried out for the period corresponding to the field observation:

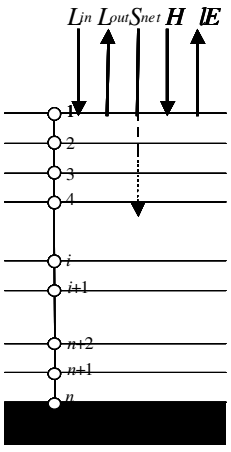

Fig. 4. A schematic sketch for one-dimensional vertical distribution of snow temperature.

from April 3, 10:00 AM to April 7, 10:00 AM. The atmospheric data for these computations were obtained from the Ward Valley weather station. The parameter values, given in Table 2, were used. A vertically homogeneous snow pack was assumed and the parameters were basically the same for any layer. An initial condition was given by the field observation, and the snow temperature at noontime was taken to be distributed uniformly with depth at zero degree. The maximum snow water content was taken as 0.05 at every depth. Homogeneous Neuman boundary condition was adopted at the bottom of the snow pack.

Fig. 5 shows the simulated snow temperature profiles. The computational results and the results of the field

Table 2
Parameter values for 1D snow temperature model

Constants and parameters	Symbol	Value
Specific heat of ice at 0 °C	C_s	2.115
Latent heat of fusion	L_f	333.5
Water content of the snow at 0 °C	W_0	0.05
Thermal conductivity of snow (J/s/cm/°C)	λ_s	0.42e−2
Penetrating radiation coefficient (1/cm)	μ	0.40
Time increment (s)	Δt	0.5
Spatial mesh size (cm)	Δz	1.0

observation (Fig. 3) are alike under the cold weather. It is almost impossible to monitor the snow surface temperatures since a sensor which would be placed on the snow surface for this purpose would be influenced by not only the snow temperature but also by air temperature and other atmospheric variables. Comparing Figs. 3 and 5, the simulated snow surface temperatures are lower than the observed ones because data at the snow surface are missing in the field observations. It should be noted that the vertical axis in Figs. 3 and 5 are not same. Fig. 5 provides information on the locations of the freezing depth. The liquid water cannot exist above the turning point of the snow temperature profile due to the cold (negative) temperature. Since the water freezing takes place mainly around the turning point, this depth is usually called the 'freezing depth'. According to the field observation and model simulation results, the assumption that a snow pack has two layers: an active layer (above the freezing depth) and an inactive layer (below the freezing depth), seems appropriate and meaningful to model the evolution of the freezing

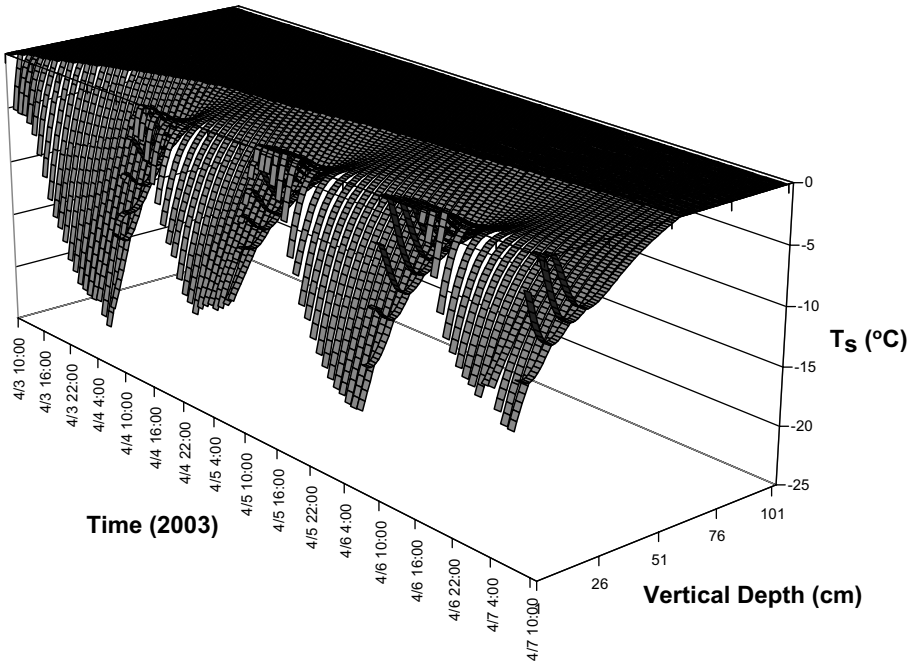

Fig. 5. Simulated snow temperature profile at every hour from April 3 to April 7. T_s indicates snow temperature.

depth with time. Also, most of the time, the snow temperature profiles in Figs. 3 and 5 look either as broken lines during nighttime or uniform during daytime. That is to say, only during a transition period, while the snow pack is being heated or chilled, the snow temperature profile seems neither linear nor uniform. Consequently, it seems appropriate to make the linear snow temperature profile assumption for the development of depth-wise integrated or point-scale model in order to focus on handling the horizontal variation of snow temperature over large horizontal distances over a watershed.

3. Linear temperature profile snowmelt model

3.1. Development of linear temperature profile snowmelt model

Based on the results of Section 2, point scale snowmelt equations with linear vertical temperature profile assumption will be derived. This linear temperature profile snow model is at point-scale, so that it can be expanded toward a distributed snow model, by means of integration of general snow equations over the depth of snowpack. Snow is composed of three phases: gas, liquid and ice, which depend on the energy balance. Morris [30] developed the general snow equations for the conservation of mass and energy within a snow pack as follows:

$$\frac{\partial}{\partial t}(\rho_k\theta_k)+\frac{\partial}{\partial z}(\rho_k\theta_k v_k)=\sum_j M_{kj}, \tag{5}$$

$$\sum_k\left[\rho_k\theta_k(C_p)_k\frac{\partial T}{\partial t}+\rho_k\theta_k v_k(C_p)_k\frac{\partial T}{\partial z}\right]=\frac{\partial}{\partial z}\left(\lambda_s\frac{\partial T}{\partial z}\right)+M_{wv}L_{wv}+M_{iw}L_{iw}+M_{iv}L_{iv}+\frac{\partial Q_n}{\partial z}, \tag{6}$$

where ρ_k is the density of component k (kg/m^3), θ_k is the volume per unit volume of snow for component k, v_k is velocity in the vertical direction for component k (m/s), t is time (s), M_{kj} is mass of component k produced per unit volume per unit time by a phase change from component j (kg/m^3 s), $(C_p)_k$ is specific heat at constant pressure of component k (kJ/kg °C), T is temperature of the mixture (°C), λ_s is thermal conductivity of snow (kJ/s m °C), Q_n is net radiation energy (kJ/m^2), L_{kj} is latent heat released by transformation M_{kj} (kJ/kg) from phase k to j, subscripts 'v', 'w', and 'i' denote vapor, water, and ice, respectively. The mass conservation consists of three equations for three phases: vapor, water, and ice.

In order to simplify the energy conservation equation, the following assumptions are made: (1) the ice matrix is stable, $v_i = 0$, (2) the heat capacity of the gaseous phase is negligible because it is very small compared to those of ice and water, $(C_p)_v = 0$ and (3) the pressure of the moist air is constant, ρ_v = const. Therefore, Eq. (6) reduces to

$$[\rho_i\theta_i(C_p)_i+\rho_w\theta_w(C_p)_w]\frac{\partial T}{\partial t}+\rho_w\theta_w v_w(C_p)_w\frac{\partial T}{\partial z}=\frac{\partial}{\partial z}\left(\lambda_s\frac{\partial T}{\partial z}\right)+M_{wv}L_{wv}+M_{iw}L_{iw}+M_{iv}L_{iv}+\frac{\partial Q_n}{\partial z}. \tag{7}$$

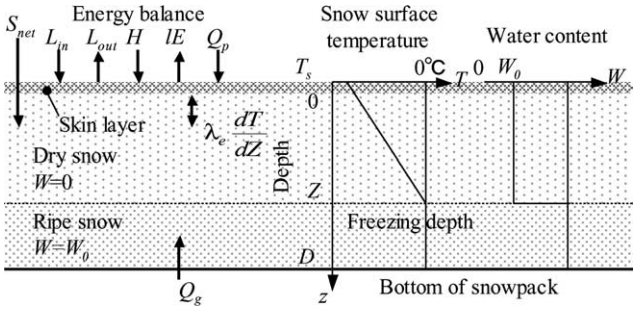

Fig. 6. Illustration of the approximation of snow temperature vertical profile.

In the developed model, a snow pack is divided into three layers in the vertical direction: a skin layer, a top active layer and a lower inactive layer, as shown in Fig. 6. The snow temperature in the upper active layer freezes below 0 °C, while the snow temperature in the lower inactive layer, below the freezing depth, stays at 0 °C. Therefore the snow temperature profile may be approximated by a straight inclined line segment in the top active layer and a straight vertical line segment in the lower inactive layer [23], as shown in Fig. 6.

In order to average the energy equation (7) with respect to depth, the Liebnitz's rule is applied to the integration of terms of Eq. (7) depthwise [17]. Performing this operation yields the depth averaged energy conservation equation as follows:

$$\rho_s C_s Z\frac{d\overline{T}}{dt}+\rho_s(C_s\overline{T}-L_f W_0)\frac{dZ}{dt}=G-M, \tag{8}$$

where

$$G=S_{net}+L_{in}-L_{out}+H-lE+Q_g+Q_p.$$

$\overline{T}$ is depth averaged snow temperature and ρ_s is depth averaged snow density. G is the energy flux available for snowmelt and for the rate of change of internal energy. S_{net} (kW) is net short-wave radiation, L_{in} and L_{out} (kW) are incoming and outgoing long-wave radiation, H (kW) is the sensible heat flux, lE (kW) is latent heat flux, Q_g (kW) is heat flux from the snow-ground interface, and Q_p (kW) is heat flux from rain. Each heat flux is estimated from meteorological information (e.g. [14]). It is noted that the energy equation in Eq. (8) may be rewritten in terms of the snow surface temperature T_s rather than the depth averaged snow temperature $\overline{T}$, due to the relationship, $T_s = 2\overline{T}$.

When the thickness of the skin layer approaches 0, the energy balance on the skin layer of the snowpack can be written as (referring to Fig. 6),

$$\lambda_s \frac{dT_s}{dZ} = L_{in} - L_{out} + H - lE + Q_p, \quad (9)$$

where λ_s (cal/cm h K) is effective thermal conductivity. It should be noted that this equation does not have a short-wave radiation term since short-wave radiation mostly penetrates the snow surface layer. To determine the effective thermal conductivity, the following empirical quadratic relationship with the snow density was proposed by Yen [44], and is used in this study;

$$\lambda_s = k_1 + k_2 \rho_s^2. \quad (10)$$

Integrating the mass conservation equations, Eq. (5), for three phases, vapor, water and ice, yields a single depth averaged mass conservation equation,

$$D\frac{d\rho_s}{dt} + \rho_s \frac{dD}{dt} = \rho_w (P_t - E - M_r), \quad (11)$$

where D (m) is thickness of snowpack, P_t (m/s) is precipitation, E (m/s) is evaporation, and M_r (m/s) is the snowmelt rate, which is determined by the snowmelt energy M in Eq. (4). Evaporation is given by

$$E = \frac{lE}{L_v \rho_w}, \quad (12)$$

where lE is latent heat flux, L_v is latent heat of vaporization, and ρ_w is density of liquid water.

The metamorphic process of snow still remains as an unknown since this process is very complicated, and the snow does not have a stationary structure. This structure is affected by atmosphere, gravity and water distribution within the snow. The snow density is the most commonly used index for the physical structure of snow. According to Horne and Kavvas [17], the snow density variation based upon the compacting and temperature gradient can be expressed as:

$$\frac{d\rho_s}{dt} = \frac{2}{3\eta_0} D\rho_s^2 e^{-0.04(T_c - T_s)} e^{-k_0 \rho_s}, \quad (13)$$

where η_0 is viscosity coefficient, a constant at 0 °C and zero density.

Snow accumulation is important for long-term snow computations, especially during the early winter. Handling of the new snowfall into the snowmelt system is explained in the following.

It is common that new snow is added to the mass in the system numerically. In this procedure, snow depth and snow density are corrected by the additional new snowfall at every computational time step when a snow pack gains new snowfall. Using this method, the snow accumulation may be expressed in the system for any time increment.

The effect of new snowfall on snow depth and snow density can also be formulated [34]. A mathematical expression for snow accumulation is useful in the development of a numerical algorithm for the snow pack evolution in time, and essential for applying other mathematical technologies to snowmelt system for further study. By adding the adjustment term of new snow accumulation to Eq. (13), the snow density equation can be written as follows:

$$\frac{d\rho_s}{dt} = \frac{2}{3\eta_0} D\rho_s^2 e^{-0.04(T_c - T_x)} e^{-k_0 \rho_s} - \frac{(\rho_s - \rho_{ns})\rho_w}{D\rho_{ns}} sn. \quad (14)$$

The effect of new snowfall on snow density appears as the second term on the right hand side of Eq. (14). It is necessary to note that a very shallow snow depth needs to be limited for the second term in Eq. (14) since this term has the state variable D in the denominator. The snow depth equation with the snow accumulation effect can be derived from the mass conservation equation (11) as:

$$\frac{dD}{dt} = \frac{\rho_w}{\rho_s}(-E - Mr + sn) - \frac{D}{\rho_s}\frac{d\rho_s}{dt}. \quad (15)$$

The snowmelt energy can be basically computed by excess energy within the energy exchanges over the snow pack, $M = G$ (refer to Eq. (8)), and snowmelt water can be calculated by Eq. (4) when snow temperature reaches as zero. Because Eq. (9), for surface gradient of snow temperature profile, vanishes with negative energy exchange En, mainly during the cooling process, a special scheme that is discussed in Appendix B, is required in order to solve this system.

3.2. Evaluation at the point location

The linear temperature profile model has been applied to Ward Creek watershed, mentioned in Section 1. The simulation period was chosen based upon the quality of available data and the data sets for the 2000–2001 and 2002–2003 observation period were chosen for the application.

Table 3 provides the list of parameters and constants used in the model simulation. The albedo, reflectance on the snow surface, is expressed as a function of surface snow age (shown in the Appendix C, Eq. (C.11)) in this study, and the constants for albedo have ranges: $k_3 = 2.31 \times 10^{-6}$–$2.89 \times 10^{-6}$, $\alpha_{min} = 0.4$–0.6, and $\alpha_{max} = 0.8$–0.9 [24]. Since rain and snow data did not exist simultaneously, it was necessary to differentiate among snow and rain within the precipitation record. The density of newly fallen snow can be estimated as a function of precipitation temperature, given in Table 4 [38], and is adopted in this study. The precipitation temperature may be estimated by means of air temperature data and the rain/snow critical temperature, a parameter that indicates the difference between air and precipitation temperature in this study.

Table 3
Constants and parameter values for linear temperature snowmelt model

Constants and parameters	Symbol	Value	Unit	Reference
Stefan–Boltzmann constant	σ	5.67e−11	kW/m^{2}K^4	E.g. Gray and Male [14]
Atmospheric emissivity	ε_s	0.99		E.g. Gray and Male [14]
Bulk coefficient for turbulent transfer	D_h	3.56e−3	kJ/m^3°C	Gray and Male [14] (Yoshida's value)
Bulk coefficient for turbulent transfer	D_e	6.62e−3	kJ/m^{3}mb	Gray and Male [14] (Yoshida's value)
Viscosity coefficient	η	20.0	cm/h	Anderson [3]
Viscosity coefficient	k_0	21.0	cm^3/g	Anderson [3]
Effective thermal conductivity coef.	k_1	2.93e−2	W/m K	Yen [44]
Effective thermal conductivity coef.	k_2	2.93e−6	W/m K	Yen [44]
Time constant for albedo	k_3	2.89e−6 [2.31e−6–2.89e−6]		Kondo et al. [24]
Converged value of albedo	α_{min}	0.56 [0.4–0.6]		Kondo et al. [24]
Maximum albedo	α_{max}	0.80 [0.8–0.9]		Kondo et al. [24]
Density of water	ρ_w	1000.0	kg/m^3	
Critical value of freezing depth	Z_{min}	0.001	m	
Water content of the snow at 0 °C	W_0	0.1		Kondo and Yamazaki [23]
Latent heat of fusion	L_f	333.5	kJ/kg	E.g. Wallace and Hobbs [43]
Latent heat of vaporization	L_V	2501	kJ/kg	E.g. Wallace and Hobbs [43]
Gas constant of vapor	R_V	461.0	J/kg°C	E.g. Berry et al. [6]
Specific heat of air at const. pressure	C_p	1.00	kJ/kg°C	Gray and Male [14]
Specific heat of water at 0 °C	C_w	4.20	kJ/kg°C	Gray and Male [14]
Specific heat of ice at 0 °C	C_s	2.115	kJ/kg°C	Gray and Male [14]
Precipitation temperature adjustment	T_{cri}	−3.0[a]	°C	
Critical snow temperature for melting	T_0	0.0	°C	
Solar constant	G_{sc}	1.367	kW/m^2	E.g. Duffie and Beckman [10]

[a] The precipitation temperature T_r may be estimated from air temperature T_a with the precipitation temperature adjustment T_{cri} because the air temperature near ground can be greater than the precipitation temperature due to temperature profile in atmosphere This value was obtained by observed SWE at the station.

Table 4
Precipitation density and percentage of snow (Susong et al. [38])

Rain temperature (°C)	Percent snow	Snow density (kg/m^3)
$T_r < -5$	100	75
$-5 \leqslant T_r < -3$	100	100
$-3 \leqslant T_r < -1.5$	100	150
$-1.5 \leqslant T_r < -0.5$	100	175
$-0.5 \leqslant T_r < 0$	75	200
$0 \leqslant T_r < 0.5$	25	250
$0.5 \leqslant T_r$	0	0

In order to gain insight as to how the developed model works, the model simulation results at the observation site point location, are shown in Fig. 7 in terms of the time series of state variables. In Fig. 7 the top graph is the input precipitation data. The second graph from the top shows the behaviors of snow surface temperature and snowmelt rate. This figure shows that snow surface temperature has a strong daily oscillation and barely achieves zero degrees Celsius until March 2003. Since the lowest snow temperature is located at the snow surface, one can see that snow melts (snowmelt shown by dashed lines on the positive axis) in the spring only when snow temperature reaches zero. The third graph from the top shows the simulated snow depth (solid line) and the location of the freezing depth (dashed line). The variation of the freezing depth synchronizes with the evolution of the snow surface temperature. The evolution of the thickness of active layer is illustrated as the snow above the freezing depth. It is shown that the thickness of the active layer is large in winter due to cold weather while the freezing depth is located near snow surface mostly during the spring. Finally, the bottom graph is the time series of the depth-averaged snow density (solid line) and of the snow surface albedo (dashed line), the most significant parameter. Although albedo is very sensitive to snowmelt, it is difficult to determine the time/space distribution of albedo. The reflectance of snow surface is expressed as an exponential function of surface snow age (Eq. (C.11)) in this study. Although the snow density is a state variable, expressed as a function of time and snow temperature, it is also affected by newly fallen snow. If there is snowfall on the old snow, the snow density at the next time step is taken as an average of densities of old snow and new snow.

Fig. 8 shows the time series of observed and model simulated snow water equivalent (SWE) at the field observation site in Ward Creek watershed, Lake Tahoe. The snow water equivalent is defined as the depth of water which would result from melting a snow pack. It is shown that the model simulation results correspond to the observed SWE at the field site location. The comparison of model simulation results against observations in Fig. 8 shows that the developed snowmelt model in this study can predict the snowmelt quite effectively during a two year period.

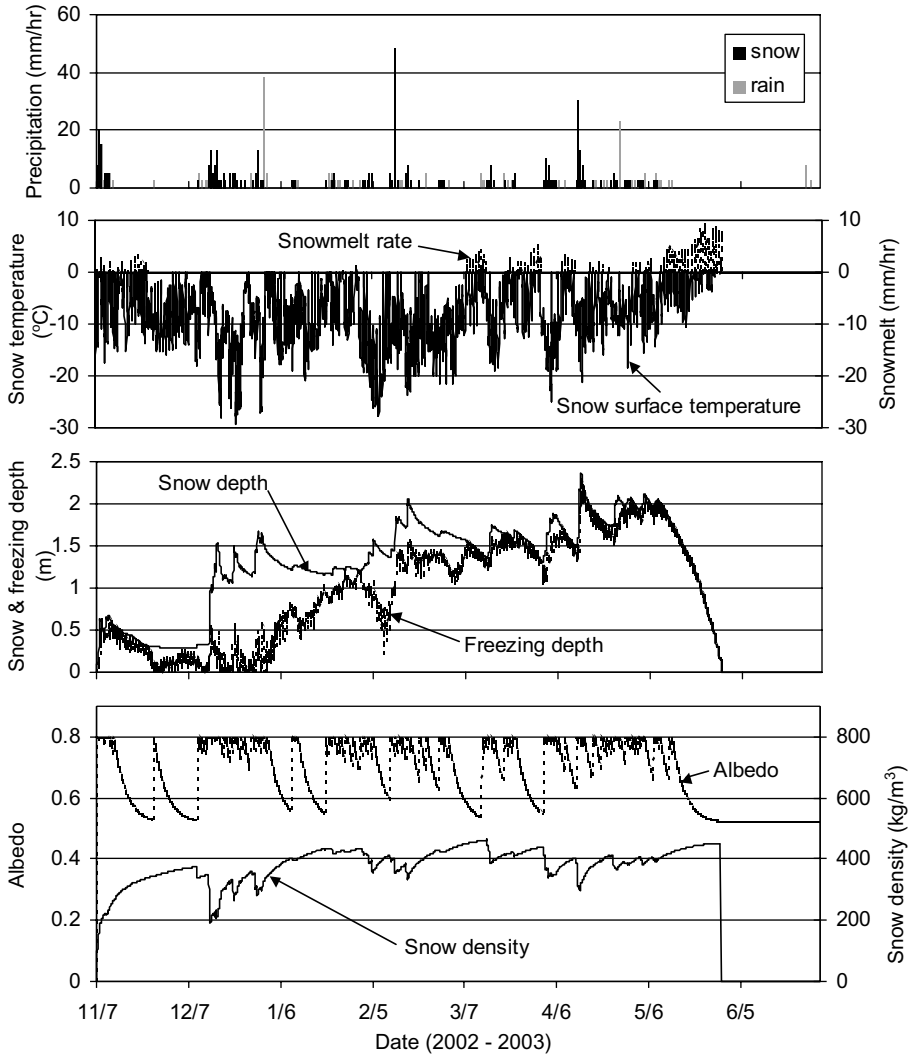

Fig. 7. Simulation results at the observation station in detail.

4. Expansion toward a spatially distributed model

4.1. Distributed snow model with linear temperature profile approximation

In this section, the point-scale snowmelt model with linear temperature profile, which was presented in Section 3, is scaled up numerically. In fact, the numerical upscaling corresponds to spatially distributed modeling, utilizing a geographical information system (GIS). This approach recently became popular with the advances in computing power ([1,28,35,46] and many others). However, this study focuses on snow physics and the effect of spatial distribution of solar (short-wave) radiation.

Fig. 9 explains the distributed snowmelt model, presented in this section. In the spatially distributed snowmelt model, all the energy components are estimated by snow physics and solar geometry. All topographic maps can be prepared in GIS, and the slope and aspect maps can be used to calculate the solar angle. At each computational node the short-wave radiation without the cloud effect is calculated by means of these maps, and the depth-averaged conservation equations for energy and mass, discussed in Section 3, are then solved. The solar geometry method for short-wave radiation is explained in Appendix C. In this manner, the effect of the land surface energy budget at every location within a modeled watershed can be accounted for.

In order to utilize the point-location-scale snow model of Section 3 to obtain spatially distributed snow predictions, one needs to use as fine a Digital Elevation Model (DEM) as possible with respect to grid size. Although with fine grid size DEM the computational time tends to become very long, by using a very fine grid DEM the effect of topography on the short-wave radiation (the prime component for snowmelt energy balance) can be represented. In this study, a 10 m $\times$ 10 m DEM which was the minimum grid size that could be

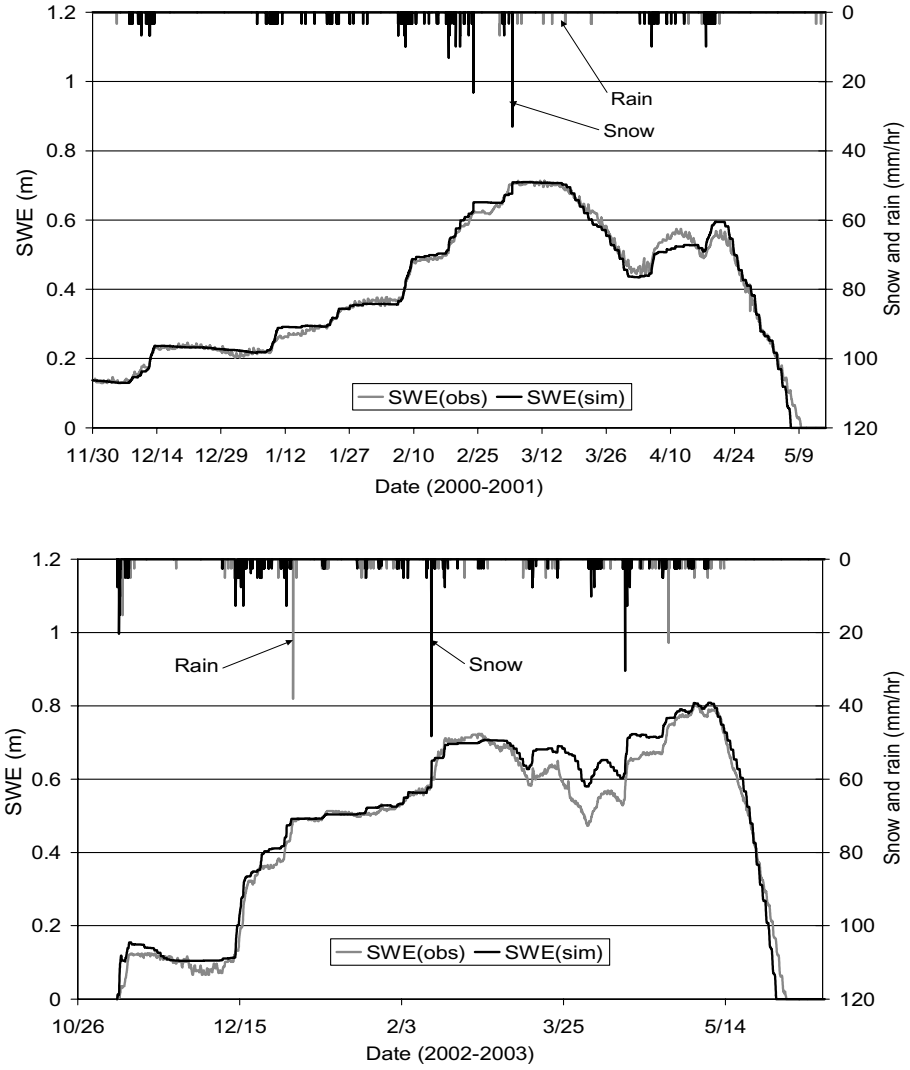

Fig. 8. Comparison of simulated and observed SWE at the field observation site.

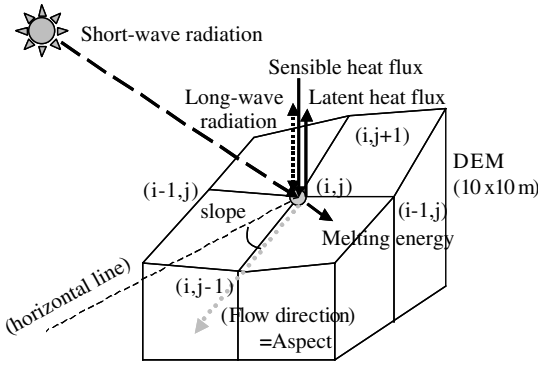

Fig. 9. Sketch of spatially distributed snow model.

obtained for the Ward Creek watershed, and a 30 m × 30 m DEM which provided acceptable computational time for the Upper Cosumnes River watershed, were used in the model applications below.

4.2. Application I: Ward Creek watershed

First model application was carried out for Ward Creek watershed, in Tahoe basin, California. The same simulation period as for the point scale application in Section 3, 2000–2001, was chosen for this application.

The boundary forcing functions, such as air temperature, relative humidity, wind velocity and precipitation, need to be spatially distributed for the model simulation. However, these forcing variables are given as input data from field observations, at a point location. Since the effect of these forcing conditions except air temperature are relatively smaller than the effect of radiation balance on snowmelt, they were considered as spatially uniform fields in this study. As air temperature may be expressed as a function of elevation, the common relationship, $z_2 - z_1 = 102(T_1 - T_2)$, (air temperature T (K), at the altitude z (m)) with atmosphere in adiabatic equilibrium was chosen to obtain spatially distributed air tempera-

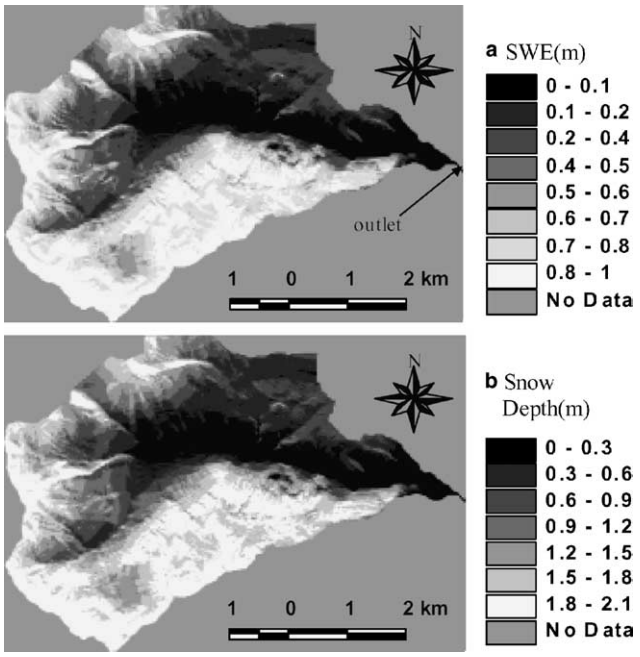

Fig. 10. Spatially distributed model simulation results over Ward creek watershed at 6:00 AM, May 5, 2001 in (a) Snow water equivalent (SWE), and (b) snow depth.

ture over the watershed (e.g. Handbook of Meteorology [6]).

Fig. 10 shows the model simulated (a) SWE, and (b) snow depth snow water equivalent as spatially distributed over Ward Creek watershed at 6:00 AM, May 5, 2001. First, one may notice in the figures for SWE and snow depth that more snow exists on the north-facing hillslopes of the watershed than the south-facing hillslopes because of the sun angle. Meanwhile, the effect of spatial variation of air temperature, which is spatially distributed with elevation over the watershed, is not pronounced in Fig. 10. This result indicates clearly that short-wave radiation, controlled by watershed topography, is the most important component of snowmelt energy balance.

4.3. Application II: Cosumnes River watershed

As a second application, the distributed snowmelt model was also applied to the Upper Cosumnes River watershed which is much larger than the Ward Creek watershed, in order to see the large-scale effects. Moreover, since the Upper Cosumnes River watershed has no field observation station, this application is to explore the potential of the snowmelt model at an ungaged basin.

As the model simulation period, 1999–2000 season was picked because of the data quality. Since all available data sources are located outside of the watershed, the observed meteorological data, air temperature, relative humidity, wind speed, and precipitation, were spatially interpolated by the inverse distance method. Only for air temperature, the effect of elevation was considered with the following procedure: (1) from the measured air temperature, the air temperature at sea level can be calculated at standard atmosphere, (2) the temperature at sea level is spatially interpolated at every computational node by inverse distance method, and (3) the spatially distributed air temperature is determined by the elevation at each computational node.

Since there is no snow survey station within the watershed, comparisons with satellite images are the only means to validate the model simulation results. Fig. 11 shows the computed SWE distribution in space on March 21, 2000 and the maximum snow extent derived with MODIS/Terra satellite images in the period from March 14 to March 21, 2000. The maximum snow extent data is assembled with the data sets of MODIS/Terra snow cover in the eight days in 500 m resolution grid since many days in winter may be covered by cloud [15]. The mixed snow cells in the bottom map may be generated in the projection transfer. This figure indicates that the spatial distribution of snow cover is modeled well since the snow-covered areas in both figures are similar. While the satellite can give information only on whether snow exists or not (snow cover extent), the model simulation can also estimate the snow depth and SWE in space.

The numerical upscaling approach is powerful in describing the effects of topography and spatially distributed information. However, it is computationally intensive. The test watershed, Ward creek, has a catchment area of 25.6 km^2 which requires 456,120 computational nodes (780×579) at the 10 m $\times$ 10 m digital elevation map resolution. The desktop computer Pentium IV processor, at 1.5 GHz speed, used in this study, spent about two days of computational time for 6 months of simulation duration. For Upper Cosumnes River watershed, because it required about three million (2485×1194) computational nodes to cover the whole region with 30 m resolution DEM, this numerical approach is computationally very intensive. The model simulation over this watershed took about 10 days as computational time with a Pentium III 1.5 GHz CPU for one-year simulation period. Furthermore, for every simulation realization with computational results given spatially at every 1000th step (1 step = 0.25 h), occupied about 1.5 GB storage in a hard drive. However, it is encouraging that these very large grid systems with very fine spatial resolution are still operable by the ordinary desktop computers. The point scale snow model with linear temperature profile approximation seems to be a convenient model for numerical upscaling of snow computations over a watershed, since the computational results described the detailed spatial distribution of snow melt-accumulation process reasonably well in the two applications.

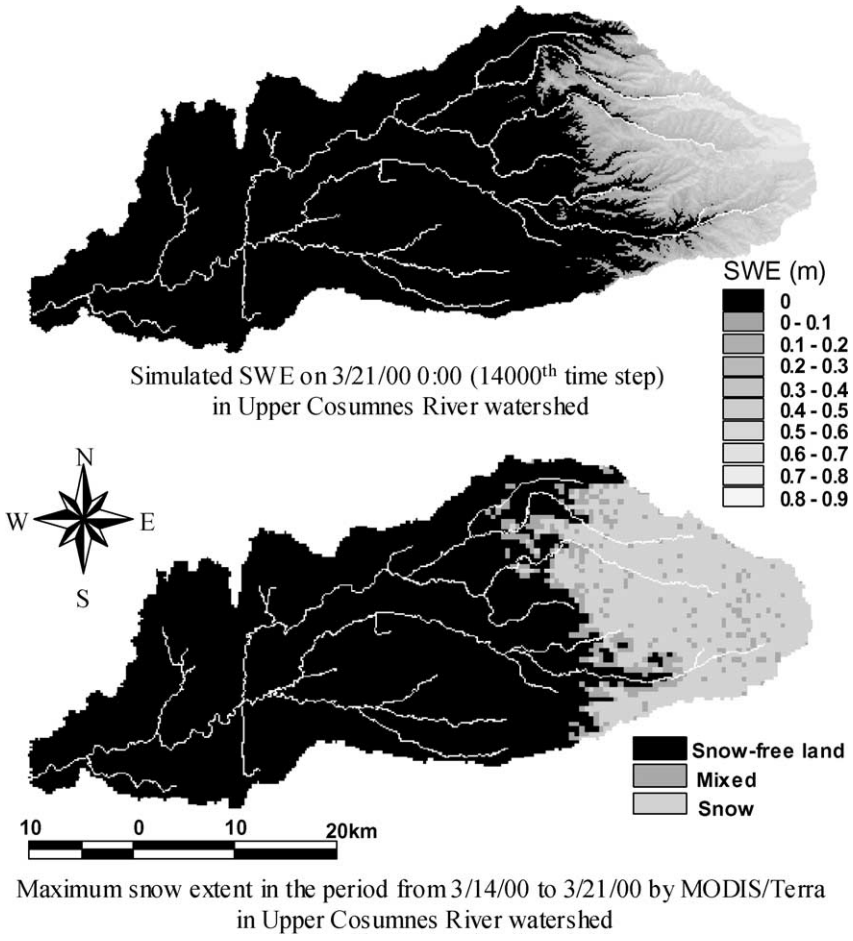

Fig. 11. Comparison between the distribution of computed SWE and snow cover data derived from satellite images [15].

5. Conclusions

The field observation on vertical snow temperature profile has been carried out at Ward Creek watershed in order to select a suitable approximation for the vertical temperature profile of a simple point scale snow model. Snow accumulation and melt processes are very complicated due to unstable snow structure and atmospheric forcing factors. It is difficult for any snowmelt model to accommodate all the effects upon the snowmelt process. If one focuses on the spatial heterogeneity of snow, a distributed snowmelt model may be an effective approach because such a model can describe the local atmospheric forcing factors well. For the spatially distributed modeling of snow process over a large watershed, it is convenient to integrate the snow process in the vertical direction, so that one can then deal only with the spatial variation of snow in the horizontal directions over the watershed. For depthwise vertical integration of the snowmelt process, selection of an approximation for the snow temperature vertical profile is the key. In the first half of this study, the snow temperature vertical profile was investigated using direct field snow temperature observations and a one dimensional snow temperature model. Both the field observations and the snow temperature model results showed that vertical snow temperature profile seems linear or exponential in shape except during the transition period from night to daytime. The analyses results confirmed the idea that a snowpack can be described in two thermal layers. The results also showed that the border of two layers, the freezing depth, varied in time as the energy level of the snowpack evolved. These results presented sufficient evidence for the development of appropriate approximations toward a simple physically based snowmelt model. The investigations on the snow temperature profile concluded that a linear temperature profile approximation may be suitable for a snowmelt model in California.

Based upon the linear temperature profile approximation, a point-scale model was developed by the depthwise integration of the general snowmelt equations given by Morris [30]. The developed snowmelt model was applied to a point location observation site in Ward

Creek watershed. It is shown that the model simulates the snow process at this site satisfactorily by taking reasonable values for its parameters. The developed model estimated the snow water equivalent at the observation site very well. As such, the physically based approximate approach to snowmelt modeling, as presented in this study, may not require significant model calibration for producing reasonable snowmelt estimates.

The distributed snow model, described here, expresses the effect of topography on the snowmelt process in detail. The point-location-scale linear temperature profile snow model has been expanded toward a spatially distributed snow model over a watershed with certain sources of spatial heterogeneity such as short-wave radiation dealt by solar geometry method. The spatially distributed snow model was applied over the whole Ward Creek watershed and Upper Cosumnes River watershed. The simulation results show clearly the fundamental influence of topography on snowmelt. The effect of topography on the snowmelt process, through its effect on solar radiation, may be quantified by the aspect and slope of the land surface as well as by elevation. The spatial simulation of snow indicated the particular significance of the aspect since the snow distribution on the north-facing hillslopes was quite different from that on the southfacing hillslopes. The distributed snow modeling, which can account for the effect of topography, seems to be a very effective way for the estimation of snowmelt at watershed scale. In Upper Cosumnes River watershed application, the computed snow spatial distribution was compared with a snow extent data derived from satellite images. Even for this ungaged basin, it was shown that the spatial coverage of snow could be reconstructed well by a spatially distributed snow model with the appropriate spatial parameter estimations.

It was shown that the spatially distributed snow model with linear temperature profile approximation could simulate snowmelt and snow depth reasonably well at any location over a watershed. Consequently, by means of the developed distributed snow model, the snowmelt water at any sub-basin can be easily computed for use as input to a watershed hydrology model.

The disadvantage of the presented approach is the heavy computational effort it requires. For a large basin or at regional scale, the computation time and the required memory and hard disk storage demands will become very large. Consequently, over large basins or regions, a spatial averaging approach to snowmelt modeling may be more appropriate in order to gain economy on computations. However, as computer processing speeds increase dramatically it seems possible that spatially distributed snowmelt models, such as the one presented here, will be able to handle snowmelt computations at watershed scale adequately in the near future.

Acknowledgements

The efforts of the second author on this study were supported partially by USEPA (R819658), Center for Ecological Health Research at U.C. Davis, and partially by USEPA Grant No. R826282010. However, the views expressed in this paper do not necessarily reflect those of the funding agencies, and no official endorsement should be inferred. The snow cover data were provided by the National Snow and Ice Data Center (NSIDC).

Appendix A. Algorithm for the numerical snow temperature model

The numerical algorithm for one dimensional snow temperature model, introduced in Section 2, is described here following Kondo and Yamazaki's [23] approach. Fig. 12 is a flowchart for the numerical algorithm on this point-location-scale model. The heat equation for snow layers may be discretized with forward Euler FD scheme for time direction and central Euler FD scheme for depth direction. Eq. (1) becomes

$$T_{s,i}^{n+1} = T_{s,i}^{n} + \frac{\lambda_s \Delta t}{C_s \rho_s (\Delta z)^2}\left(T_{s,i-1}^{n} - 2T_{s,i}^{n} + T_{s,i+1}^{n}\right) + \frac{\Delta t}{C_s \rho_s}\left\{\mu S_{net} e^{(-\mu z)} - L_f M_{r,i}^{n}\right\}. \quad (A.1)$$

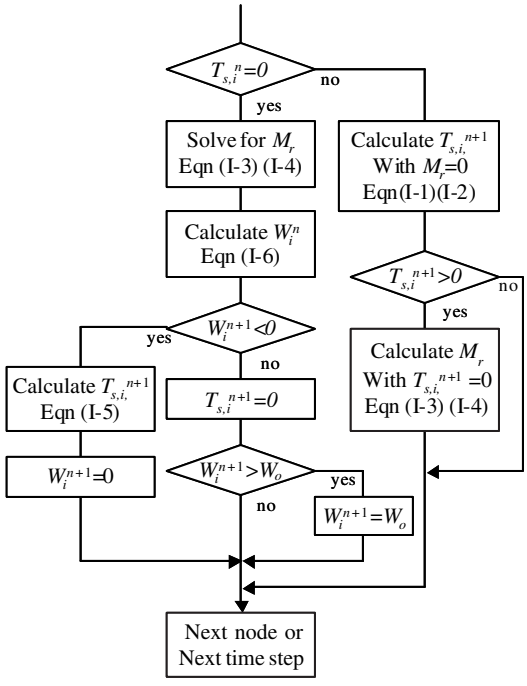

Fig. 12. Flowchart of 1D snow temperature model.

And, at a skin (surface) layer, Eq. (2) may be rewritten as

$$T_{s,1}^{n+1} = T_{s,1}^{n} + \frac{\lambda_s \Delta t}{C_s \rho_s (\Delta z)^2}(T_{s,2}^{n} - T_{s,1}^{n}) + \frac{\Delta t}{C_s \rho_s}\{\mu S_{net} e^{(-\mu z)} - L_f M_{r,1}^{n}\} + \frac{\Delta t}{C_s \rho_s \Delta z}(L_{in} - L_{out} - lE + H), \quad (A.2)$$

where Δz is displacement in depth direction (m), Δt is time increment (s), ρ_s is density of snow (kg/m^3) at depth z, T_s is snow temperature (°C), and M_r is snowmelt rate (m/s).

Superscript n indicates time step and subscript i means location, numbered from snow surface. S_{net} (kW) is net short-wave radiation, L_{in} and L_{out} (kW) are incoming and outgoing long-wave radiation, H (kW) is the sensible heat flux, lE (kW) is latent heat flux. C_s is specific heat of snow; and λ_s is heat conductivity of snow. is the extinction coefficient of solar radiation within the snow cover. When snow temperature reaches zero, extra energy is consumed for snowmelt. The energy equations, (A.2) and (A.3), may be arranged for snowmelt rate $M_{r,i}$:

$$M_{r,i}^{n+1} = -C_s \rho_s \frac{T_{s,i}^{n+1} - T_{s,i}^{n}}{L_f \Delta t} + \lambda_s \frac{T_{s,i-1}^{n} - 2T_{s,i}^{n} + T_{s,i+1}^{n}}{L_f (\Delta z)^2} + \frac{\mu}{L_f} S_{net} \exp(-\mu z). \quad (A.3)$$

For the surface boundary:

$$M_{1}^{n+1} = -C_s \rho_s \frac{T_{s,1}^{n+1} - T_{s,1}^{n}}{L_f \Delta t} + \lambda_s \frac{T_{s,2}^{n} - T_{s,1}^{n}}{L_f (\Delta z)^2} + \frac{\gamma}{L_f} S_{net} \exp(-\gamma z) + \frac{L_{in} - L_{out} - lE + H}{L_f \Delta z}. \quad (A.4)$$

For the cooling process, the snow temperature needs to depart from zero when water content W goes to a negative number, since negative snow water content indicates that no more water exists to freeze. The snow temperature for first step of cooling process can be calculated by

$$T_{s,i}^{n+1} = \frac{W_i^{n} \rho_s L_f}{C_s}. \quad (A.5)$$

The snow water content WC can be computed by Eq. (A.6) obtained from mass conservation equation (3) at each layer;

$$WC_i^{n+1} = WC^{n} + \frac{\Delta t M_{r,i}^{n}}{\rho_s} - Q \Delta t. \quad (A.6)$$

Appendix B. Algorithm for the point-location-scale linear temperature profile snowmelt model

The numerical solution of the developed point-location-scale snowmelt model was modified from Kondo and Yamazaki [23] and is used in this study. Fig. 13 is a flow chart of the solution algorithm. An important feature for the solution of this system is the assumption that snowmelt occurs only when critical snow temperature (0 °C) realizes on the snow surface. In other words, the freezing depth reaches zero (snowpack surface) whenever snowmelt takes place. Then, when the freezing depth, Z, reaches the snow surface, the snow surface temperature T_s acts as a constant (critical temperature) and the system can be solved for four state variables: snowmelt energy, snow density, snow depth, and freezing depth. Otherwise, the system can be solved for another set of state variables: snow surface temperature, snow density, snow depth, and freezing depth, because of no snowmelt.

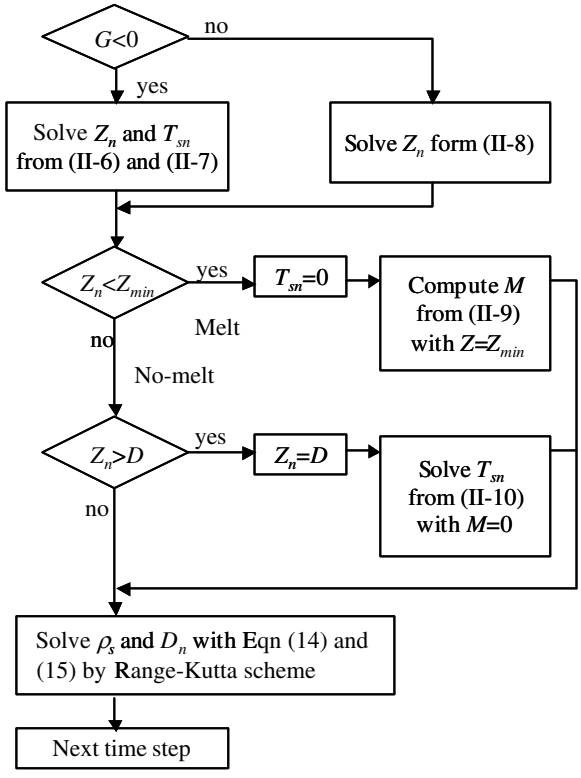

Fig. 13. Flowchart for point-location-scale snow model with linear temperature profile in the vertical direction.

The energy conservation equation (10) for the snowpack may be rewritten as follows:

$$\frac{1}{2} C_s \rho_s \frac{dZ T_s}{dt} - W_0 \rho_s L_f \frac{dZ}{dt} = G - M, \quad (B.1)$$

where

$$G = S_{net} + L_{in} - L_{out} + H - lE + Q_g + Q_p. \quad (B.2)$$

Applying forward Euler finite difference scheme to Eq. (B.1), one can obtain the following form that is exactly the same form as in Kondo and Yamazaki [23]:

$$\frac{1}{2}C_s\rho_s[Z(T_0 - T_s) - Z_n(T_0 - T_{sn})] + W_0\rho_s L_f(Z - Z_n) = G\Delta t - M\Delta t, \quad (B.3)$$

where T_0 is the critical melting temperature of snow, T_s and T_{sn} are snow surface temperature respectively at current and next time steps, Z and Z_n are freezing depths respectively at current and next time steps, M is the melting energy, G is energy balance over the snowpack at the new time step, and Δt is time increment. Another energy equation can be written for the heat balance of a snow surface. Hence, the Eq. (7) may be written as,

$$\lambda_s\frac{T_{sn} - T_0}{Z_n} = L_{in} - L_{out} + H - lE + Q_p. \quad (B.4)$$

Combining Eqs. (B.3) and (B.4) with the formulations of every energy exchange component yields the following quadratic equation:

$$A_2Z_n^2 + A_1Z_n + A_0 = 0, \quad (B.5)$$

where

$$A_2 \equiv C_1\lfloor 0.92\times 10^{-5}\sigma T_a^6 - \varepsilon\sigma T_a^4 + C_2(T_a - T_0) - D_eU_ze^*(T_a)(1-h)\rfloor - C_2C_3,$$
$$A_1 \equiv [C_3Z + C_1Z(T_0 - T_s) - G\Delta t]C_2 - C_3\lambda_s,$$
$$A_0 \equiv \lambda_s[C_3Z + C_1Z(T_0 - T_s) - G\Delta t],$$
$$C_1 \equiv \frac{1}{2}C_s\rho_s,$$
$$C_2 \equiv 4\varepsilon\sigma T_a^3 - D_HU_z + D_eU_z\left[\frac{\partial e^*}{\partial T}\right]_{T_a},$$
$$C_3 \equiv W_0\rho_s l_f.$$

The solution of Eq. (B.5) can be obtained easily. Therefore, when snow surface temperature is below zero Celsius degree, one can calculate the freezing depth with

$$Z_n = \frac{-A_1 - (A_1^2 - 4A_2A_0)^{1/2}}{2A_2}. \quad (B.6)$$

Then, with calculated freezing depth, the snow surface temperature T_{sn} can be determined by solving the energy equation (B.3) as follows:

$$T_{sn} = T_0 - \frac{1}{Z_n}\left[Z_0(T_0 - T_s) + \frac{1}{C_1}\{-G\Delta t + M\Delta t + C_3(Z - Z_n)\}\right]. \quad (B.7)$$

However, when the heat balance at the surface layer is positive, the energy conservation equation at the surface layer vanishes (it is assumed that the snow surface temperature cannot be positive even with finite freezing depth). In the case of positive heat balance, only the energy conservation equation over the snowpack, Eq. (B.3), should be solved for Z_n with $T_{sn} = 0$ without M rather than solving both Eqs. (B.3) and (B.4):

$$Z_n = Z + \frac{C_1Z(T_0 - T_s) - G\Delta t}{C_3}. \quad (B.8)$$

As a result, when the freezing depth is less than a very small value like 1 mm, the snow melts. The snowmelt energy is then computed by solving the energy balance Eq. (B.3) of snowpack for M:

$$M = G - \frac{1}{\Delta t}[C_1\{Z(T_0 - T_s) - Z_n(T_0 - T_{sn})\} + C_3(Z - Z_n)]. \quad (B.9)$$

When the freezing depth Z is greater than the snowpack depth, then only the heat balance equation for the entire snowpack (B.3) is used to calculate the snow surface temperature T_{sn},

$$T_{sn} = \frac{Z_n(0.92\times 10^{-5}\sigma T_a^6 - \varepsilon\sigma T_a^4) + Z_n\{C_2T_a - D_eU_ze^*(1-h)\} - \lambda T_0}{C_2Z_n + \lambda}. \quad (B.10)$$

Appendix C. Estimation of solar radiation

The purpose of this section is to explain how to calculate the short-wave radiation from the sun as a function of location, land surface aspect and slope, day of the year, and time of day. First of all, solar position must be predicted. It is defined on Duffie and Beckman [10], Iqbal [19] and others.

Fig. 14 explains the annual variation of solar angle and distance between sun and earth. One can then calculate an extraterrestrial solar radiation S_0 on the surface normal to the sun by means of the solar constant, $S_{SC} = 1367$ (W/m^2), as

$$S_0 = S_{SC}E_0, \quad (C.1)$$

where E_0 is an eccentricity correction factor of earth's orbit that can be calculated with calendar day.

Solar declination δ (rad) is the angle between the polar axis and the normal to the ecliptic plane. Solar declination is a function of day of the year and it can be modeled by an appropriate function such as Spencer's expression [36].

Fig. 15 defines hourly varying angles to represent the position of the sun. Solar zenith angle θ_0 (rad) on the horizontal surface can be calculated by

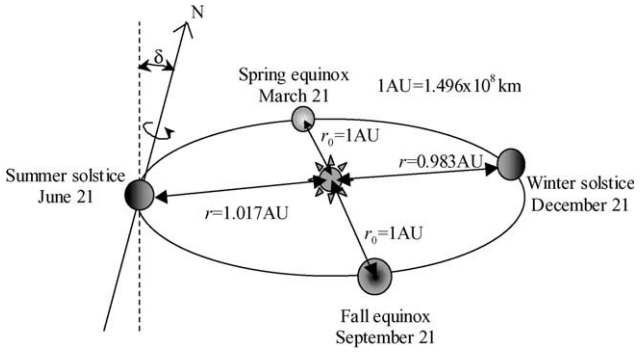

Fig. 14. Annual variation of solar location.

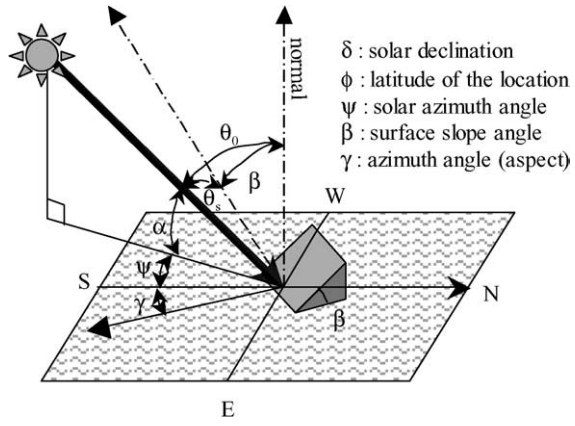

Fig. 15. Definition of angles that express location of the sun on the slope.

$$\cos\theta_0 = \sin\delta\sin\phi - \cos\delta\cos\phi\cos\omega, \tag{C.2}$$

where δ is solar declination, ϕ is latitude of the location, and ω is hour angle. The hour angle is an angle between the observer's meridian and solar meridian, which is zero at noon and positive in the morning. It changes 15 degrees per hour. The hour angle is given as

$$w = \frac{\pi}{12}(\text{solar times} - 12). \tag{C.3}$$

Therefore, the solar altitude or solar elevation α (rad) is written as

$$\alpha = \frac{\pi}{2} - \theta_0. \tag{C.4}$$

Since the surface of a snowpack is usually not horizontal in a mountainous region, the effects of slope and aspect of surface need to be considered in order to estimate shortwave radiation flux. Solar illumination angle on the slope, θ_s, is calculated by the following equation:

$$\cos\theta_s = \cos\theta_0\cos\beta + \sin\theta_0\sin\beta\cos(\phi - \gamma), \tag{C.5}$$

where β is a surface slope angle, and γ is azimuth angle (aspect) of the land or snowpack surface. All of the angles, necessary for the calculation of the solar position, are thus obtained.

Next, the effect of the atmosphere is discussed. There are several ways to predict how much radiation is transmitted, absorbed or reflected from the top of the atmosphere to land surface on a clear day. However, in practice, simple modeling, such as ASHRAE [12] and Hottel's model [18], is usually sufficient to avoid long computational times. In this study Hottel's model, introduced in [10], was chosen since the effect of elevation on snowmelt should be considered in mountainous regions.

The beam radiation can be calculated by the extraterrestrial solar radiation, G_o, and transmittance of atmosphere, τ_b:

$$G_b = \tau_b G_o. \tag{C.6}$$

There are several expressions for the transmittance of the atmosphere, and most of them are in exponential form. Hottel's expression for transmittance is a simple exponential function.

Diffuse radiation (isotropic, circumsolar and horizontal diffusion) may be expressed by [26]

$$G_d = \tau_d G_o, \tag{C.7}$$

$$\tau_d = 0.271 - 0.294\tau_b. \tag{C.8}$$

Thus, the total short-wave radiation on a horizontal surface can be obtained as follows:

$$G_T = G_b\frac{\cos\theta_s}{\cos\theta_0} + G_d\left(\frac{1+\cos\beta}{2}\right). \tag{C.9}$$

Eq. (C.9) expresses the incoming short-wave radiation on the snowpack, S_{in}.

Another important factor that affects the incoming short-wave radiation is albedo, α, as most of the radiation is reflected from the snow surface. The net short-wave radiation, S_{net}, is written as:

$$S_{net} = S_{in}(1-\alpha). \tag{C.10}$$

In this study, the albedo is expressed as a function of time. The reflectance of snow decreasing exponentially with time, is obtained from the experimental results of Kondo et al. [24]:

$$\alpha = \alpha_{min} + (\alpha_{max} - \alpha_{min})\exp(-n_s k_3), \tag{C.11}$$

where α is albedo as function of the time from the last snowfall, α_{min} is the asymptotic value of albedo, α_{max} is maximum albedo corresponding to new snow, k_3 is time constant, and n_s is the age of snow.

References

[1] Abbott MB, Bathurst JC, Cunge JA, O'Connell PE, Rasmussen J. An introduction to European Hydrological Systém—Système Hydrologique Européen (SHE), 1. History and philosophy of a physically-based distributed modeling system, 2. Structure of a physically-based distributed modeling system. J Hydrol 1986;87(1–2):45–77.

[2] Anderson EA. Development and testing of snow pack energy balance equations. Water Resour Res 1968;4(1):19–37.
[3] Anderson EA. A point energy and mass balance model of a snow cover, NOAA Technical Report NWS 19. US Department of Commerce (Washington DC) 150, 1976.
[4] Amorocho J, Espildora B. Mathematical simulation of the snow melting processes. USA: Department of Water Science and Engineering, University of California, Davis; 1966.
[6] Berry FA, Bollay E, Beers NR. Handbook of meteorology. New York: McGraw-Hill Book Company, Inc.; 1945.
[8] Blöschl G, Kirnbauer R. Point snowmelt models with different degrees of complexity—internal processes. J Hydrol 1991;129: 127–47.
[10] Duffie JA, Beckman WA. Solar engineering of thermal processes. John Wiley & Sons, Inc.; 1991.
[11] Dune SM, Colohan RJE. Developing the snow component of a distributed hydrological model: a step-wise approach based on multi-objective analysis. J Hydrol 1999;223:1–16.
[12] Farber EB, Morrison CA. Clear-day design values. In: Jordan RC, Liu BY editors. In applications of solar energy for heating and cooling of building. ASHRAE GRP-170. New York, 1977.
[14] Gray DM, Male DH. Handbook of snow. Canada: Pergamon Press; 1981.
[15] Hall DK, Riggs GA, Salomonson VV. MODIS/Terra Snow Cover 8-Day L3 Global 500m Grid V004. February to March 2000. Boulder, CO, USA: National Snow and Ice Data Center. Digital media. 2000, updated weekly.
[17] Horne FE, Kavvas ML. Physics of the spatially averaged snowmelt process. J Hydrol 1997;191:179–207.
[18] Hottel HC. A simple model for estimating the transmittance of direct solar radiation through clear atmospheres. Solar Energy 1976;18:129–34.
[19] Iqbal M. Introduction to solar radiation. Canada: Academic Press; 1983.
[20] Jordan R. A one dimensional temperature model for a snow cover. Technical documentation for SNTHERM.89, US Army Corps of Engineers, Cold Region Research Laboratory, Hanover, New Hampshire, 1991.
[23] Kondo J, Yamazaki T. A prediction model for snowmelt, snow surface temperature and freezing depth using a heat balance method. J Appl Meteorol 1990;29:375–84.
[24] Kondo J, Numata Y, Yamazaki T. Parameterization of snow albedo. J Jpn Soc Snow Ice 1988;50:216–24 (in Japanese).
[25] Kuchment LS, Gelfan AN. Dynamic-stochastic model of snowmelt runoff generation and its application for estimating extreme floods. Proceedings of the Annual Eastern Snow Conference 2001;58:373–88.
[26] Liu BYH, Jordan RC. The interrelationship and characteristic distribution of direct, diffuse and total solar radiation. Solar Energy 1960;4(3):1.
[27] Marks D, Kimball J, Tingey D, Link T. The sensitivity of snowmelt process to climate conditions and forest cover during rain-on-snow: a case study of the 1996 Pacific Northwest flood. Hydrol Process 1998;12:1569–87.
[28] Marks D, Domingo J, Susong D, Link T, Garen D. A spatially distributed energy balance snowmelt model for application in mountain basins. Hydrol Process 1999;13:1935–59.
[30] Morris EM. Modeling the flows of mass and energy within a snowpack for hydrological forecasting. Ann Glasiol 1983;4.
[31] Morris EM. Snow and ice. In: Anderson M, editor. Hydrological Forecasting. Chichester: Wiley; 1985. p. 154–82.
[33] Obled C, Rosse B. Mathematical models of melting snowpack at an index plot. J Hydrol 1977;32:139–63.
[34] Ohara N. Numerical and stochastic upscaling of snowmelt process, PhD dissertation, Dept. of Civil Eng., University of California, Davis, USA, 2003.
[35] Pomeroy JW, Gray DM, Shook KR, Toth B, Essery LR, Pietroniro A, et al. An evaluation of snow accumulation and ablation processes for land surface modeling. Hydrol Process 1998;23:2339–67.
[36] Spencer JW. Fourier series representation of the position of the sun. Search 1971;2(5):172.
[37] Sugawara M. Run-off analysis method. Tokyo: Kyoritsu syuppan; 1972 (in Japanese).
[38] Susong D, Marks D, Garen D. Methods for developing time-series climate surfaces to drive topographically distributed energy- and water-balance models. Hydrol Process 1999;13:2003–21.
[40] US Army Corps of Engineers. Snow Hydrology (Portland, Oregon), Plate 8-1, 1956.
[43] Wallace MJ, Hobbs VP. Atmospheric Science: An Introductory Survey. San Diego: Academic Press inc.; 1977.
[44] Yen YC. Effective thermal conductivity of ventilated snow. J Geophys Res 1962;67:1091–8.
[46] Zhang Z, Kane DL, Hinzman LD. Development and application of a spatially-distributed Arctic hydrologic and thermal process model (ARHYTHM). Hydrol Process 2000;14:1017–44.